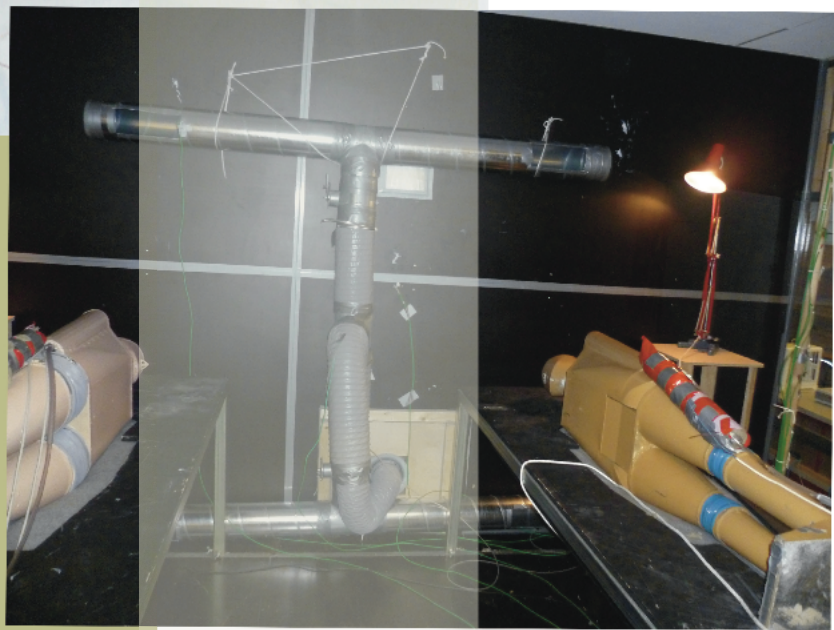
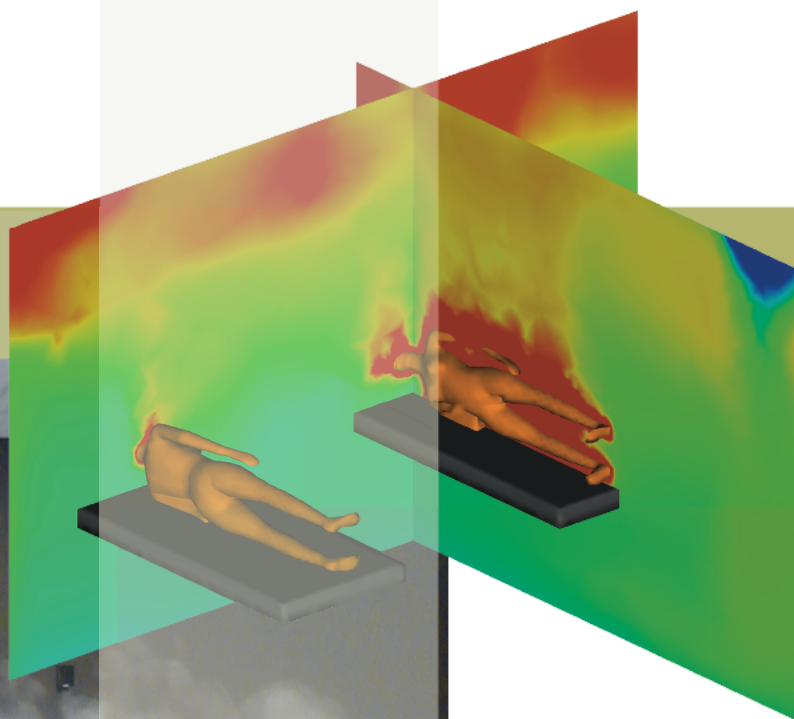


Cross infection in hospital wards

Farzad Khalegi
Anders Møllerskov



Appendix

Contents

A	Calibration of equipment	3
A.1	Calibration of thermocouples type k	3
A.2	Calibration of artificial lungs	3
B	Heatbalance	5
C	Reproduction of results	7
D	Diffusers	8
E	Obtaining the right measuring period	10
F	Computational Fluid Dynamics	11
F.1	Discretization	17
F.2	Convergence	19
F.3	Relaxation factor	20
G	Particle distribution	22
H	Procedure of particle measurements	26
I	Calculation on minute volume used in measurements	28

Calibration of equipment

The equipment used for the measurements have to be calibrated in order to get correct values. All equipment used have been calibrated but not all of it will be described. In the following is the calibration of the thermocouples type k and the artificial lungs described.

A.1 Calibration of thermocouples type k

The thermocouples are calibrated for two temperatures which is the range that is expected to measure in. The two temperatures are approximately $10^{\circ}C$ and $40^{\circ}C$. The reason why only two temperatures are used is because the calibration equation obtained is a linear equation and other points at for instance $25^{\circ}C$ would be on the same line.

The calibration is carried out by setting a temperature on the *VENUS 2410B plus* so the *AΣΛ F200* shows a temperature close to the desired temperature of either $10^{\circ}C$ or $40^{\circ}C$. The temperatures are logged on a *GRANT 1250 series*. The logger is set to take samples every 30 seconds and it logs for a minimum of five minutes which gives at least ten samples. The temperature on the *AΣΛ F200* is not logged but it is recorded manually every 30 seconds. The average of the values measured and recorded is used to make the calibration equations.

A.2 Calibration of artificial lungs

Two artificial lungs are use in the experiment. They are constructed and operated in different ways. One of them have a chamber with a piston. The cylinder in which the piston goes up and down has a diameter of $125mm$ and the maximum stroke length of the piston of $110,5mm$ giving it a volume of $1,36l$. The volume can be controlled by decreasing the length of the piston stroke, this can be done manually by turning a bolt. A frequency of $10min^{-1}$ was desired but this was not obtainable instead is a frequency of $8min^{-1}$ obtained as that was the highest possible if a airflow of $6l/min$ where to be used. The frequency is controlled by turning a valve. The other artificial lung is made of a compressor which sucks in air and blows it out afterwards. The flow is controlled by a button, by turning that the flow can be decided it has a fluent control meaning it operates within an interval. The frequency of the exhalation is also controlled by a button but the lung has five preinstalled settings for the frequency. When calibrating the frequency the equipment is positioned at some level and it is counted how many time it exhales per minute. When calibrating the

flow is device used which measures the total amount of air which is blown into it. The lungs exhaled for half a minute and it was checked how much air it exhaled during that time. The frequency of this lung is set at 10min^{-1} with a flow of $6\text{l}/\text{min}$. It was experienced that the lung with the compressor gave completely different result with regard to air flow compared to what the control on the equipment suggested.

Appendix B

Heatbalance

To ensure that the air temperature and air change rate is within a reasonable range a heat balance calculation is made. The heat balance for the test room is made using equation B.1:

$$\Phi_{Ventilation} + \Phi_{Transmission} + \Phi_{Internal} = 0 \quad (\text{B.1})$$

Where:

$\Phi_{Ventilation}$	Heat exchange from ventilation [W]
$\Phi_{Transmission}$	Heat exchange from transmission [W]
$\Phi_{Internal}$	Heat exchange from internal loads [W]

The heat exchange due to the ventilation can be calculated when the mean inlet air temperature and mean air temperature in the room is known. The heat exchange due to transmission through surfaces is assumed to be close to zero as it is attempted to keep the same temperature in the test room and the laboratory. Equation B.1 can be reduced to:

$$q \cdot \rho \cdot c(T_{Room} - T_{inlet}) + 0 + \Phi_{Internal} = 0 \quad (\text{B.2})$$

Where:

q	Air flow to the room [m^3/s]
ρ	Air density [kg/m^3]
c	Heat capacity [$J/kg^\circ C$]
T_{Room}	Temperature of the room air [$^\circ C$]
T_{inlet}	Temperature of the inlet air [$^\circ C$]

The internal heat loads for the different set ups are as described in section ???. It is assumed the air density and heat capacity of the inlet air and room is the same. This is not completely true but the difference is very small. The density and heat capacity of the air is chosen for $20^\circ C$. The indoor air temperature is chosen within a range which is acceptable for the users due to their activity level but the temperature also has to be very close to the temperature of

the surroundings in order to make the assumption of no heat exchange to the surroundings valid. The ACH should be chosen within a range that guaranties an acceptable atmospheric indoor environment for the cases with the standing manikins. For the measurements with the manikins lying in bed the ACH is chosen in the range given by the centers for Disease Control and Prevention, a low and a high ACH is chosen in order to see the influence of the ACH on the personal exposure index. In table B is listed the ACH chosen for the different set ups.

Set up	Calculated ACH [h^{-1}]	Actual ACH [h^{-1}]
One standing manikin	4,8	3,5
Micro environment between two standing persons	6,1	3,5
Hospital ward low ACH	5,2	5,4
hospital ward high ACH	10,2	10,1

Reproduction of results

In order to guarantee the results obtained are of good quality and not just coincidental, extra measurements were made of some of the cases to show the results can be reproduced. The replica was not made right after the first one so it is more like one long case, other case were run in between so the outside conditions are not the same. A comparison of the personal exposure indexes and the Archimedes number justifies that the results are valid the values are listed in table C.1.

Case	Personal exposure index	Archimedes number
12	1,97	68,6
12a	2,07	73,6
13	2,41	35,1
13a	2,71	46,8

Table C.1: Listed is personal exposure indexes and Archimedes numbers for original and replica measurements.

As seen in table C.1 there is not large differences between the original and the reproduction. It can be concluded that the results can be reproduced and that they therefore are valid.

Appendix D

Diffusers

In this section is a description of the inlet and outlet diffusers, how they are designed and what kind of flow patterns is observed.

D.0.1 Inlet diffuser

The inlet diffusers are made of textile. There are two of them and the dimensions of each of the diffusers are $60\text{cm} * 120\text{cm}$ giving a total inlet area of 0.144 m^2 . The inlet diffuser can be seen in figure D.1.



Figure D.1: The inlet diffuser mounted in the ceiling.

The large surface area enables them to deliver a lot of air to the room without creating draft. This is a very good ability since a high ACH in the room reduces the risk of cross infection. When making the measurements with the standing manikins, both the study with one standing manikin and the two standing manikins, it was expected that the air from the inlet diffuser would flow along the surface close to it and thereby utilize the Coanda effect. When the inlet is located close to the wall and the manikins are located underneath it, two different flow patterns are seen dependent on where the manikins are located. When the manikins are located under the inlet diffuser as in case 7 and case 8 as seen in figure D.2 the inlet air

follows the wall as if it uses the the Coanda effect but it seems as if it is the thermal plume of the manikins which "push" the inlet air jet to that side.

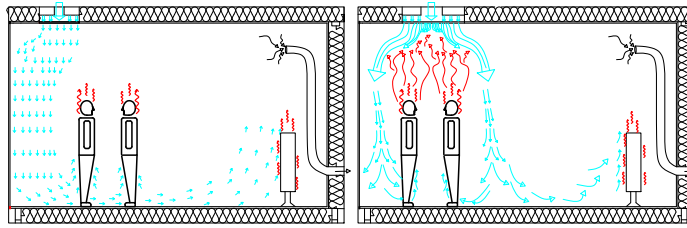


Figure D.2: Airflow observed around manikins.

This tendency is emphasized by the fact that the inlet air flow sometimes shifted from flowing along the wall and going to the other side when case 8 is run.

It is observed that the air rises from the floor level and up whenever it reaches a warm surface. This is also expected as the cold air on the floor is entrained into the thermal plume of the manikin.

D.0.2 Outlet diffuser

There are used two different designs of exhaust openings during this part of the project. The outlet diffuser is in the case with standing manikins a round opening with a diameter of 160 *mm* as the influence of the exhaust is not investigated. For the cases with two manikins laying in bed is one of the main objectives to look at the influence of the exhaust opening. The diffuser is made in a way where it is possible to have different openings opened at the same time, the two top openings, the two bottom openings or all four openings. The exhaust can be seen in figure D.3



Figure D.3: The exhaust opening is located in the background.

Obtaining the right measuring period

In order to ensure that time of measurements are sufficient a test has been performed. The set up chosen for the test is case 5, where two manikins are facing each other with a mutual distance of 110cm. In this case the inlet diffuser is located in the middle of the room and the manikins stands to left of the diffuser. Before the test is started the room already contains tracergas from another case, so the room do not have to be filled up with gas but currents have to be changed. In table E.1 can the average and peaks of the measurements be seen for three different sampling channels.

Measuring time	Channel 1		Channel 2		Channel 3	
	Average [ppm]	Peak [ppm]	Average [ppm]	Peak [ppm]	Average [ppm]	Peak [ppm]
Two hours	150	241	171	296	191	276
Four hours	148	241	162	296	232	832
Six hours	147	241	163	296	219	832
Eight hours	145	241	164	296	220	832
Ten hours	147	241	167	296	220	832
Eleven and a half hours	150	276	167	296	218	832

Table E.1: Comparison of different time steps.

From table E.1 it can be seen that the average values after two hours of measurements are quite close to the values after eleven and a half hours, but the peak values have not occurred yet for two of the three channels. After four hours of measuring the average values are still close to those after eleven and a half and the peak values are close to those acquired after eleven and a half hours. The time of each measurement is therefore set at a minimum of four hours as that time is regarded as sufficient to guarantee a average and peak value sufficiently close to the value acquired after eleven and a half hours of measurement. Another reason why four hours of measurements is used is because of the number of channels used. The more channels used the longer time between each reading of gas concentrations and in order to guarantee sufficient data to make a reliable average, sampling in more than two hours is needed.

Computational Fluid Dynamics

Basically the prediction of the air flow is based on a solution of the fundamental flow equations. For a total description of the flow, eight differential equations which are coupled and non-linear must be solved;

- Continuity equation
- Momentum equation for x, y and z directions
- Energy equation
- Transport equation
- Equation for turbulent kinetic energy
- Equation for dissipation of turbulent kinetic energy

Since the cases presented in the report are steady state, the time dependency can be eliminated from the governing equations. However the full equation system will be shown in the following.

F.0.3 Continuity Equation

The continuity equation can be described under the assumption that the amount of fluid entering the control volume is the same as the amount leaving the control volume, F.1 and furthermore that the fluid is incompressible.

$$\frac{\partial \rho}{\partial t} + \nabla \cdot (\rho \vec{u}) = S_m \quad (\text{F.1})$$

where

- ρ is the density of the fluid
- u is the velocity
- S_m is the source term

F.0.4 Momentum Equations

The momentum equation for describing the flow velocity in the volume is expressed by Newton's 2nd Law of Motion F.2.

$$\frac{\partial}{\partial t} (\rho \vec{u}) + \nabla (\rho \vec{u} \vec{u}) = -\nabla p + \nabla (\vec{\tau}) + \rho \vec{g} + \vec{F} \quad (\text{F.2})$$

where

- ρ is the fluid density
- u is the velocity
- p is the static pressure
- $\vec{\tau}$ is the stress tensor
- ρg is the gravitational body force
- F is the external body force and user defined source terms
-

The stress tensor $\vec{\tau}$ is described as $\mu[(\nabla \vec{u} + \vec{u}^T) - \frac{2}{3} \nabla \vec{u} I]$ This equation is solved for each axis in the volume, resulting in three equations.

F.0.5 Turbulence modeling

A method that can be employed to render the Navier-Stokes equations tractable so that the small-scale turbulent fluctuations do not have to be directly simulated is the Reynolds-averaging. This method introduces additional terms in the governing equations that need to be modeled in order to achieve a 'closure' for the unknowns. The Reynolds-averaged Navier-Stokes (RANS) equations govern the transport of the averaged flow quantities, with the whole range of the scales of turbulence being modeled. One of the closure models that is available is the $K-\varepsilon$ models. In Reynolds averaging, the solution variables in the instantaneous Navier-Stokes equations are decomposed into the mean and fluctuating components. Confer F.3

$$u_i = \bar{u}_i + u'_i \quad (\text{F.3})$$

where

- \bar{u}_i is the mean velocity component
- u'_i is the fluctuating velocity component

Similarly for other scalar quantities F.4

$$\varphi = \bar{\varphi} + \varphi' \quad (\text{F.4})$$

φ can be replaced by scalars such as pressure, energy or species concentrations. By substituting this form for the flow variables into the instantaneous continuity and momentum equations and then taking a time average yields the time averaged momentum equations F.0.5.

$$\frac{\partial \rho}{\partial t} + \frac{\partial}{\partial x_i}(\rho u_i) = 0$$

$$\frac{\partial}{\partial t}(\rho u_i) + \frac{\partial}{\partial x_j}(\rho u_i u_j) = -\frac{\partial p}{\partial x_i} + \frac{\partial}{\partial x_j} \left[\mu \left(\frac{\partial u_i}{\partial x_j} + \frac{\partial u_j}{\partial x_i} - \frac{2}{3} \delta_{ij} \frac{\partial u_l}{\partial x_l} \right) \right] + \frac{\partial}{\partial x_j}(-\overline{\rho u'_i u'_j})$$

These equations are called Reynolds Averaged Navier Stokes(RANS) equations. The difference between this equation and the instantaneous Navier Stokes is that the velocities and other solution variables are now representing time averaged values. Also additional terms now appear and they represent the effects of turbulence. These Reynolds stresses, $-\overline{\rho u'_i u'_j}$, must be modeled in order to close the equation F.0.5. Furthermore the Reynolds averaged approach to turbulence modeling requires that the Reynolds stresses in F.0.5 need to be appropriately modeled. For this reason a common method which employs the Boussinesq hypothesis is used. In here the Reynolds stresses are related to the mean velocity gradients see F.0.5.

$$-\overline{\rho u'_i u'_j} = \mu_t \left(\frac{\partial u_i}{\partial x_j} + \frac{\partial u_j}{\partial x_i} \right) - \frac{2}{3} \left(\rho k + \mu_t \frac{\partial u_k}{\partial x_k} \right) \delta_{ij}$$

In the RNG $k-\varepsilon$ model which originally is a branch of the $k-\varepsilon$ model the above mentioned Boussinesq hypothesis is used because of the advantage that less computational cost is associated with the computation of the turbulent viscosity, μ_t . In the case of the $k-\varepsilon$ models, two additional transport equations for the turbulence kinetic energy, k , and the turbulence dissipation rate, ε , and μ_t is computed as a function of k and ε .

Another parameter that plays an important role is the terms of computation. Meaning that each turbulent model require time in order to solve the turbulence transport equations. Due to the extra terms and functions in the governing equations and a greater degree of non-linearity, computations with the RNG $k-\varepsilon$ model tend to take 10-15 % more CPU time than with the standard $k-\varepsilon$ model. This disadvantage is how ever counter balanced because besides the time per iteration, the choice of turbulence model can affect the ability to obtain a converged solution. For instance, the standard $k-\varepsilon$ model is slightly over-diffusive in certain situations, while the RNG $k-\varepsilon$ model is designed such that the turbulent viscosity is reduced in response to high rates of strain. Strain is a measure of the amount of deformation that occurs when an object is placed under stress. Strain rate is defined as the change in strain over the change in time.

Furthermore in the derivation of the $k-\varepsilon$ model, the assumption is that the flow is fully turbulent, and the effects of molecular viscosity are negligible. The standard $k-\varepsilon$ model is therefore valid only for fully turbulent flows. In the contrary, RNG $k-\varepsilon$ turbulent model are given some improvements such as

- Additional term in the diffusion equation that significantly improves the accuracy for rapidly strained flows.
- The effects of swirl on turbulence which enhances the accuracy for swirling flows.
- Analytic derived differential formula for effective viscosity that accounts for low-Reynolds number effects.(Effective treatment of the near wall region is needed)

On the basis of these improvements the RNG- k - ε model is used as the turbulent model for the present CFD predictions in this study.

In the RNG- k - ε model there are two transported variables, where the first is the turbulent kinetic energy, K , F.5 which determines the energy in the turbulence, and the turbulent dissipation ε , F.6 which determines the scale of the turbulence. Mathematically these two can be described as follows

$$\frac{\partial}{\partial t}(\rho k) + \frac{\partial}{\partial x_i}(\rho k u_i) = \frac{\partial}{\partial x_j} \left(\alpha_k \mu_{eff} \frac{\partial k}{\partial x_j} \right) + G_k + G_b - \rho \varepsilon - Y_M + S_k \quad (F.5)$$

and

$$\frac{\partial}{\partial t}(\rho \varepsilon) = \frac{\partial}{\partial x_j} \left(\alpha_\varepsilon \mu_{eff} \frac{\partial \varepsilon}{\partial x_j} \right) + C_{1\varepsilon} \frac{\varepsilon}{k} (G_k + C_{3\varepsilon} G_b) - C_{2\varepsilon} \rho \frac{\varepsilon^2}{k} - R_\varepsilon + S_\varepsilon \quad (F.6)$$

where

- ρ is the fluid density
- k is the turbulence kinetic energy
- u is the velocity
- μ_{eff} is the dynamic viscosity
- α_k is the inverse Prandtl number for k
- α_ε is the inverse Prandtl number for ε
- G_k is the production of turbulence kinetic energy due to mean velocity gradients
- G_b is the production of turbulence kinetic energy due to buoyancy
- Y_M is the dilatation dissipation
- $C_{1\varepsilon}$ is a constant 1.42
- $C_{2\varepsilon}$ is a constant 1.68
- $C_{3\varepsilon}$ is a constant -

The constant $C_{3\varepsilon}$ defined as F.7;

$$C_{3\varepsilon} = \tanh \frac{v}{u} \quad (\text{F.7})$$

where

- v is the component of the flow velocity parallel to the gravitational vector
- u is the component of the flow velocity perpendicular to the gravitational vector

Y_M is a compressibility modification or the contribution of the fluctuating dilatation in compressible turbulence to the overall dissipation rate.

G_k and G_b describe the generation of turbulence by momentum and gravitational forces respectively and is described as follows F.8 and F.9;

$$G_k = -\overline{\rho u'_i u'_j} \frac{\partial u_j}{\partial x_i} \quad (\text{F.8})$$

and

$$G_b = \beta g_i \frac{\mu_t}{Pr_t} \frac{\partial T}{\partial x_i} \quad (\text{F.9})$$

where

- β is the thermal expansion coefficient for the fluid
- g is the gravitational force
- Pr_t is the turbulent Prandtl number
- μ_t is the turbulent viscosity

As mentioned, in the RNG k - ε turbulence model an additional term is added in the dissipation equation for turbulent kinetic energy. It follows that this extra term in the dissipation equation improves the accuracy for rapid strained flows. This equation can be described as F.10;

$$R_\varepsilon = \frac{C_\mu \rho \eta^3 (1 - \eta/\eta_0) \varepsilon^2}{1 + \beta \eta^3} \frac{1}{k} \quad (\text{F.10})$$

where

- η is defined as Sk/ε
- η_0 is 4.38
- β is 0.012

This additional term distinguishes RNG k - ε with k - ε .

F.0.6 Energy Transport Equation

The energy equation, F.11 describes the energy balance for each cell and shows the temperature distribution in the model. The outcome from this equation system gives rise to low residuals, whereas the convergence criterion for this equation is lower than for other governing equations. The energy equation contains elements describing the flow of the air, as well as the species included in the cell. Thus this equation is more crucial in buoyant flows where the flow is determined by the temperature distribution in the model.

$$\frac{\partial}{\partial t} (\rho E) + \nabla (\vec{u} (\rho E + \rho)) = \nabla \left(\lambda_{eff} \nabla T - \sum h_j \Gamma_j + (\tau_{eff} \vec{u}) \right) + S_h \quad (\text{F.11})$$

where

- $\lambda_{eff} \nabla T$ is the energy transfer due to thermal conductivity
- $\sum h_j \Gamma_j$ is the species diffusion of species j
- E is the energy term
- $\tau_{eff} \vec{u}$ is the viscous dissipation

Furthermore the energy term E is described as F.12

$$E = h - \frac{P}{\rho} + \frac{u^2}{2} = \sum Y_j h_j + \frac{u^2}{2} \quad (\text{F.12})$$

where

- Y_j is the mass fraction of species j
- u is the velocity
- h_j is the expression, F.13

$$h_j = \int_{T_{ref}}^T c_{p,j} dT \quad (\text{F.13})$$

where $c_{p,j}$ is the thermal conductivity for the fluid.

F.0.7 Species Transport Equation

The species transport equation, F.14 contains description on the production of species in that particular cell, which can either be through chemical reactions or by a predefined source term. Furthermore the equation describes the dissipation of species within that particular cell.

$$\frac{\partial}{\partial T} (\rho Y_j) + \nabla (\rho \vec{u} Y_j) = -\nabla \vec{\Gamma}_j + R_j + S_j \quad (\text{F.14})$$

where

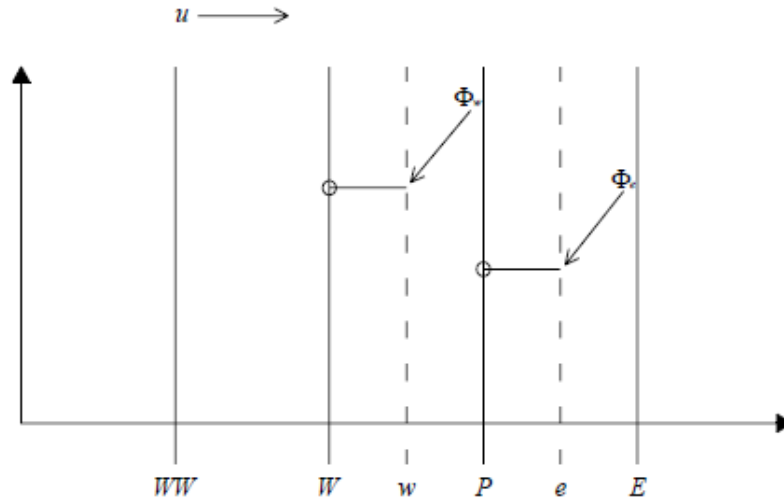
- R_j is the net rate of production of species j by chemical reaction
- S_j is the rate of creation by addition from the dispersed phase plus any user-defined sources
- Γ_j is the dissipation of species j
- Y_j is the mass fraction of species j

F.1 Discretization

Discretization concerns the process of transferring continuous models and equations into discrete counterparts. By using the control volume method, each of the governing equations represented can be converted into algebraic equations. Subsequently these can be solved numerically. In the present study first and second order upwind schemes are utilized. These two schemes are then used for discretizing the momentum equation, energy equation, species and turbulence equations.

F.1.1 First order upwinded scheme

The advantages and disadvantages of this scheme are accounted for in the present study. The advantage of this scheme is that it makes fast calculations and can be used as an initial study of the results attained from the simulation. There is however a higher risk of numerical diffusion when using the First-Order Upwind Scheme in more complex models with higher turbulent airflows. Numerical diffusion is a difficulty with computer simulations of continuous systems such as fluids and an possible explanation could be that in Eulerian simulations, time and space are divided into a discrete grid and the continuous differential equations of motion, such as the Navier-Stokes equation are discretized into finite-difference equations. The discrete equations are in general more diffusive than the original differential equations, so that the simulated system behaves differently than the intended physical system. so in general the First-Order Upwind Scheme is used for laminar flow in a model, modeled with a grid consisting mainly of quadrilateral or hexahedral grid cells, as this decreases the risk of numerical diffusion when the flow is parallel to the grid lines. The mode of operation of the First-Order Upwind Scheme is shown in figure F.1.1. The center value for the cell is assumed to be the average value throughout the entire cell, cell P, and when calculating the value for the neighboring cell, cell E, the face value of cell E is equal with the center value cell P.

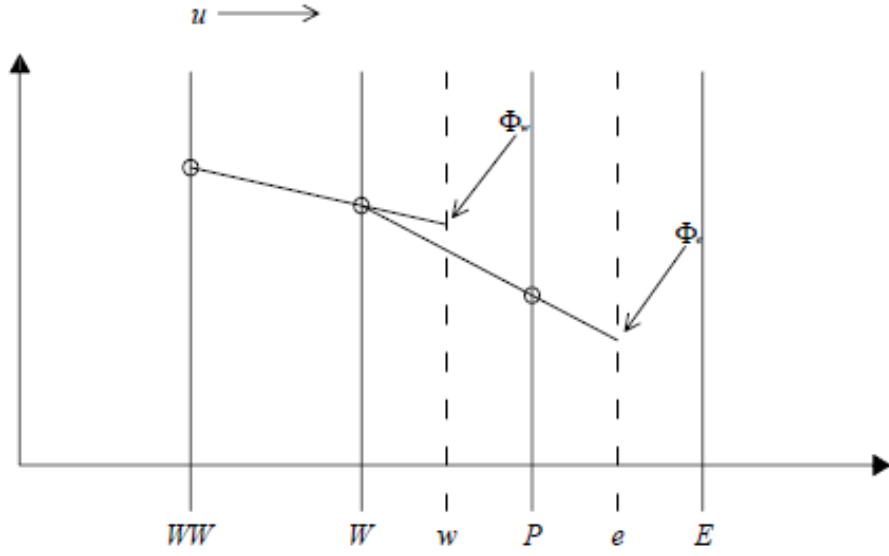


In order to illustrate how the First-Order Upwind Scheme works, an example is shown to clarify this discretization. The example is taken from a simple 2D-case where the governing equation is as shown F.1.1 and solved;

$$\begin{aligned} \frac{\partial}{\partial x}(\rho u_x \phi) + \frac{\partial}{\partial y}(\rho u_y \phi) &= \frac{\partial}{\partial x} \left(\Gamma \frac{\partial \phi}{\partial x} \right) + \frac{\partial}{\partial y} \left(\Gamma \frac{\partial \phi}{\partial y} \right) \\ \rho u_x \frac{(\phi_E - \phi_W)}{dx} + \rho u_y \frac{(\phi_N - \phi_S)}{dy} &= \Gamma \frac{\phi_E + \phi_W - 2\phi_P}{dx^2} + \Gamma \frac{\phi_N + \phi_S - 2\phi_P}{dy^2} \\ 2\Gamma(dy^2 + dx^2)\phi_P &= dy^2(\rho u_x dx - \Gamma)\phi_W + dy^2(-\rho u_x dx - \Gamma)\phi_E \dots \\ &+ dx^2(\rho u_y dy - \Gamma)\phi_N + dx^2(-\rho u_y dy - \Gamma)\phi_S \end{aligned}$$

F.1.2 Second order upwind scheme

In order to achieve more accurate results, a second order upwind scheme is used. This scheme is more suitable for more complex airflows, but in expense of abstruse convergence achievement as the equation system includes more variables for each grid point when solving the equations. This can be illustrated by reviewing the previous example and implement the second order upwind scheme to solve the discretized equations. The enhancement of this scheme can be explained as this model tends to include the influence of not only the neighboring point but also the previous point at cell WW when calculating the results for cell P, see figure F.1.2 and F.1.2



$$\begin{aligned} \frac{\partial}{\partial x}(\rho u_x \phi) + \frac{\partial}{\partial y}(\rho u_y \phi) &= \frac{\partial}{\partial x} \left(\Gamma \frac{\partial \phi}{\partial x} \right) + \frac{\partial}{\partial y} \left(\Gamma \frac{\partial \phi}{\partial y} \right) \\ \rho u_x \frac{(\phi_e - \phi_w)}{dx} + \rho u_y \frac{(\phi_n - \phi_s)}{dy} &= \Gamma \frac{\phi_e + \phi_w - 2\phi_P}{dx^2} + \Gamma \frac{\phi_n + \phi_s - 2\phi_P}{dy^2} \\ (3\rho dx dy (u_x dy + u_y dx) + 4\Gamma (dy^2 + dx^2)) \phi_P &= dy^2 (4\rho u_x dx + \Gamma) \phi_w + (-\rho u_x dx dy^2) \phi_{ww} + \Gamma dy^2 \phi_E \dots \\ &+ dx^2 (4\rho u_y dy + \Gamma) \phi_s + (-\rho u_y dx^2 dy) \phi_{ss} + \Gamma dx^2 \phi_N \end{aligned}$$

F.2 Convergence

CFD problems in general are non-linear, and the solution techniques use an iterative process to successively improve a solution, until convergence is reached. The exact solution to the iterative problem is unknown, but it is desirable to be sufficiently close to the solution for a particular required level of accuracy. Convergence therefore does need to be associated with a requirement for a particular level of accuracy. Convergence is often measured by the level of residuals, the amount by which discretized equations are not satisfied, and not by the error in the solution. Convergence can be hindered by a number of factors. Large numbers of computational cells, overly conservative under-relaxation factors, and complex flow physics are often the main causes. Sometimes it is difficult to know whether a converged solution is obtained. During the present CFD predictions the residuals are monitored. The previous example on figure F.1.1 on the facing page is reviewed. The residuals are calculated, see figure F.2.

$$\begin{aligned}
 a_P \phi_P &= a_W \phi_W + a_E \phi_E + a_N \phi_N + a_S \phi_S \\
 2\Gamma(dy^2 + dx^2)\phi_P &= dy^2(\rho u_x dx - \Gamma)\phi_W + dy^2(-\rho u_x dx - \Gamma)\phi_E \dots \\
 &\quad + dx^2(\rho u_y dy - \Gamma)\phi_N + dx^2(-\rho u_y dy - \Gamma)\phi_S \\
 a_P &= \sum_{nb} a_{nb} - S_P \\
 R_P &= \sum_{nb} a_{nb} - a_P - S_P \\
 R_P &= dy^2(\rho u_x dx - \Gamma) + dy^2(-\rho u_x dx - \Gamma) + dx^2(\rho u_y dy - \Gamma) \dots \\
 &\quad + dx^2(-\rho u_y dy - \Gamma) - 2\Gamma(dy^2 + dx^2)
 \end{aligned}$$

Positive values of a_p and a_{np} are desired and for this reason the examples shown above, see F.2 need modifications with respect to grid spacing. In Fluent the default values are 0.001 for most of the governing equations except the energy equation. For the energy equation convergence is achieved when the residuals for this equation has much lower values, below $1 \cdot 10^{-6}$. The residuals calculated for each governing equation for the entire domain is calculated as F.15.

$$R^\varphi = \frac{\sum_{domain} |\sum_{nb} a_{nb} \varphi_{nb} - a_p \varphi_p - S_p|}{\sum_{domain} |a_p \varphi_p|} \quad (\text{F.15})$$

F.3 Relaxation factor

Each of the variables(mass,mom,density) represents an equation the solver is trying to solve. Each iteration the values obtained for the variables should get closer and closer together, converge. For simple problem the default values can be used. Sometimes for many reasons the solution can become unstable so a relaxation factor is used, here it takes part of value from previous iteration to dampen solution and cut out steep oscillations. This can be expressed as follows F.16

$$\varphi_{update} = \varphi_{old} + \alpha \Delta \varphi \quad (\text{F.16})$$

where

- φ_{update} is the updated value which is put into the governing equation
- φ_{old} is the old value entered in the governing equation
- $\Delta \varphi$ is the computed difference between the old and new value
- α is the relaxation factor

F.3. Relaxation factor

The disadvantage of the relaxation factors are that they sometimes tend to slow down the computational time. A solution to this is to run the simulations with the default relaxation values and change if the solution can become unstable.

Particle distribution

A more detailed distribution of the particle distribution on the floor is illustrated in this section. Graphs are made for each case. The way to read the graph is the distance from the manikin is in *cm* on the x-axis but also the percentage of each particle size with the vertical line in the distance counting as zero per cent. on the y-axis is the particle size in μm .

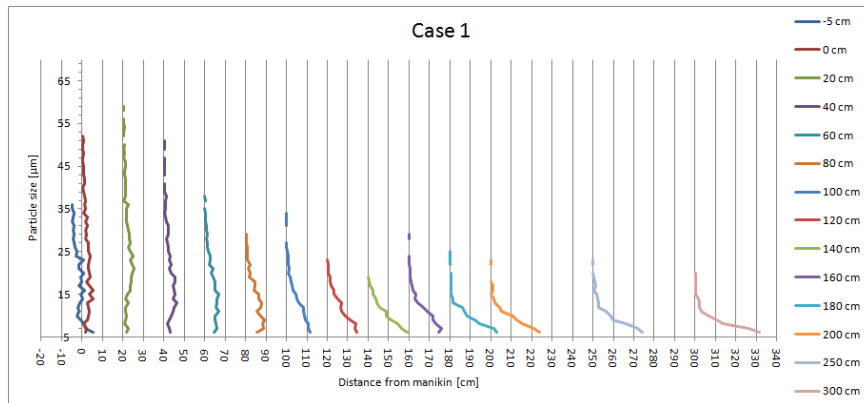


Figure G.1: The particle distribution for case 1.

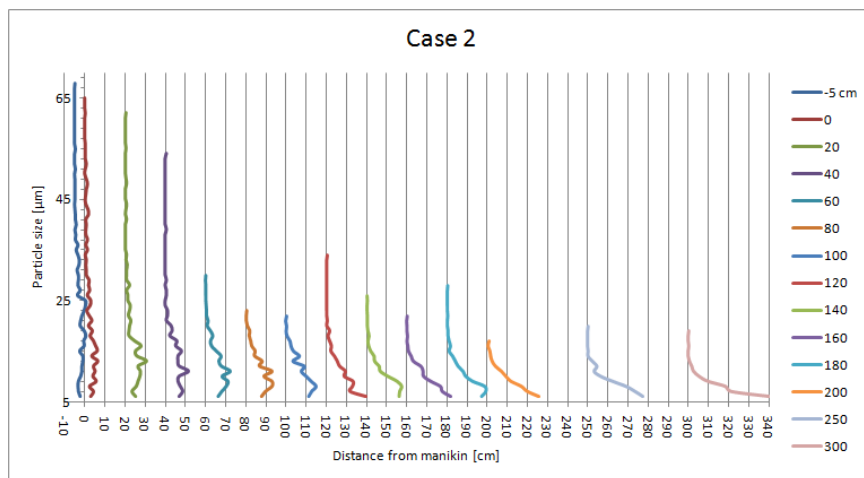


Figure G.2: The particle distribution for case 2.

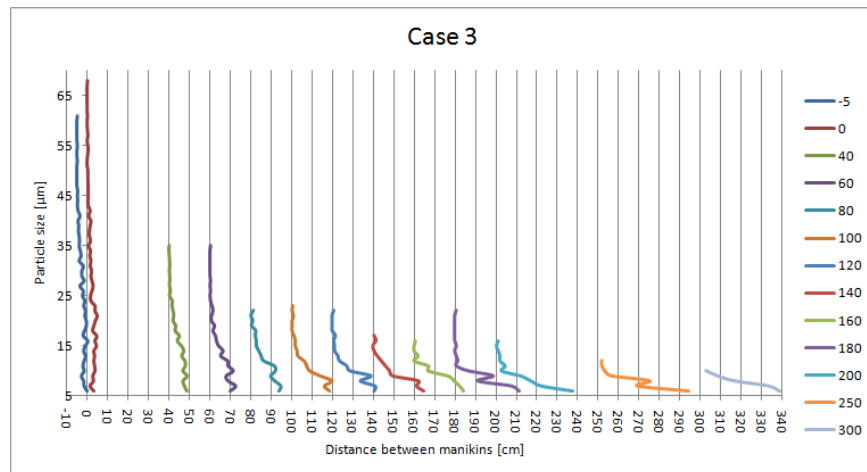


Figure G.3: The particle distribution for case 3.

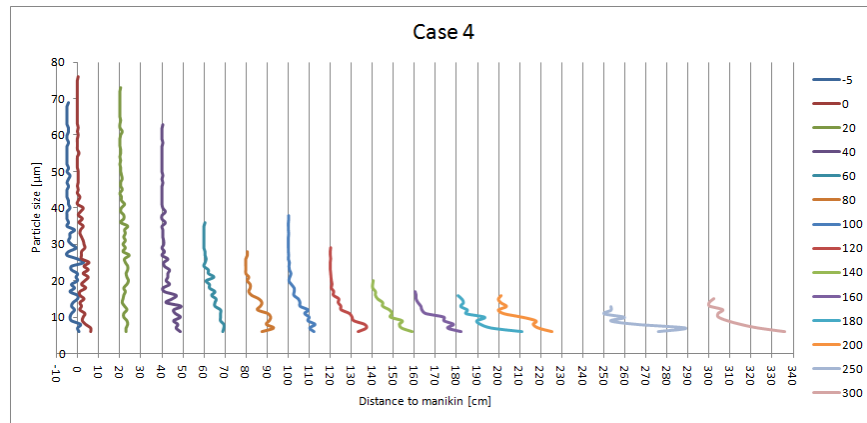


Figure G.4: The particle distribution for case 14

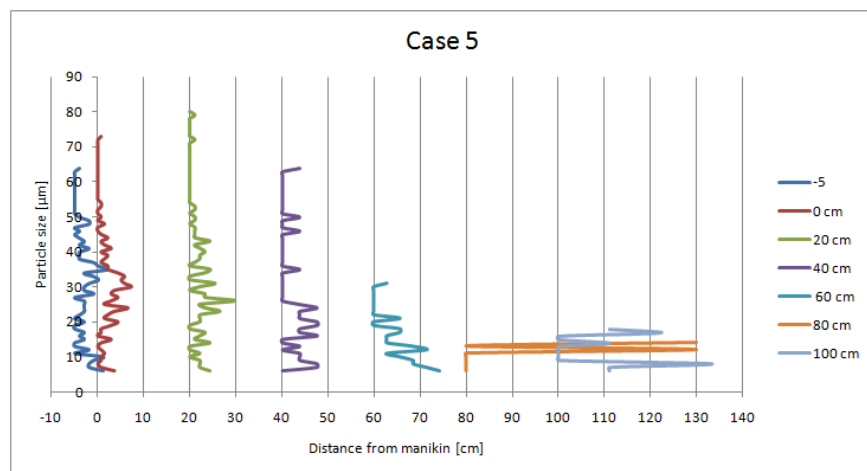


Figure G.5: The particle distribution for case 5.

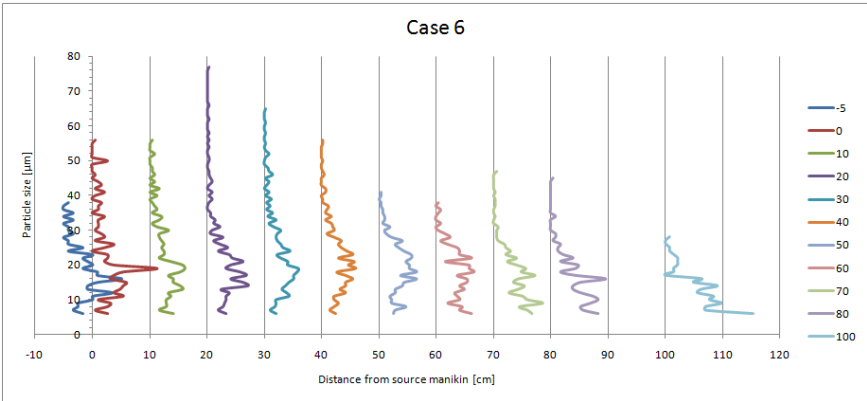


Figure G.6: The particle distribution for case 6.

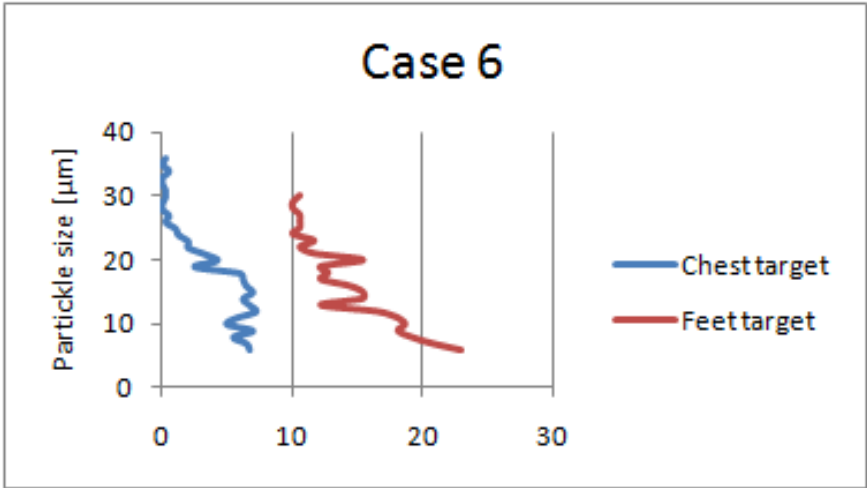


Figure G.7: The particle distribution for case 6 at the chest and feet of the target.

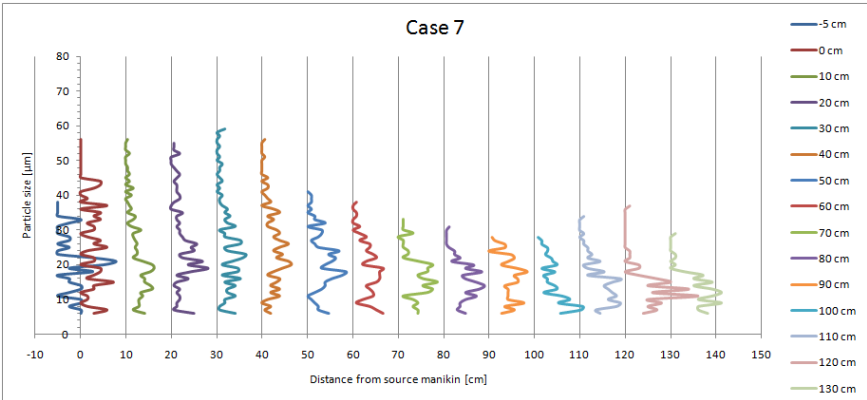


Figure G.8: The particle distribution for case 7.

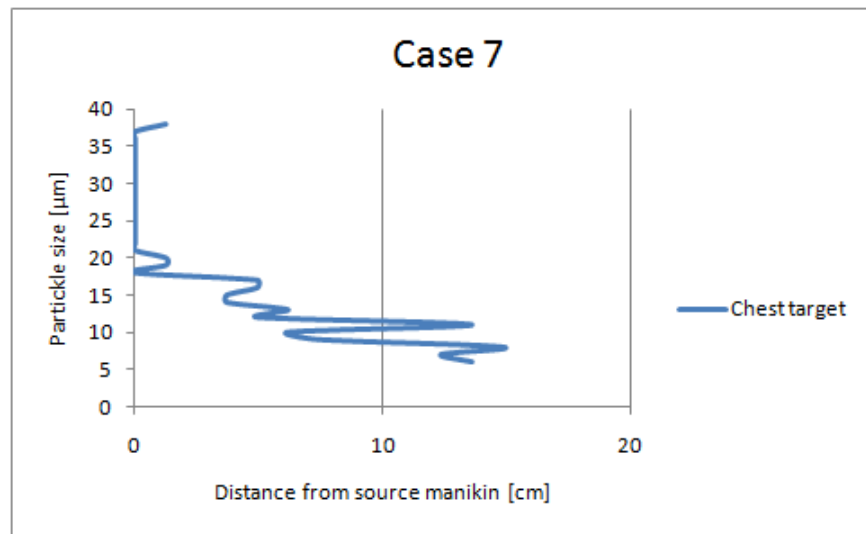


Figure G.9: The particle distribution for case 7 at the chest of the target.

Procedure of particle measurements

In this section is the procedures concerning the measurements of particles explained. Before each measurement is the room air cleaned as much as possible this is done by letting the ventilation system run from the end of one measurement to the beginning of the next. For the first measurements this period of time was an entire night but when time was an issue the room where ventilated for at least three hours. Particles are also vacuumed around and on the manikin so it is easier to see where the particles deposit on and around the manikin. While the ventilation system is running are the heat adjusted for the manikin and exhalation air, this is done in order to make steady state conditions shorter. When the air is cleaned as well as possible black cardboard is placed on the glass platform. The reason for the glass platform were to make sure the floor is completely even, but the glass is a bit uneven and the cardboard is not completely even either. The cardboard is placed after the particle are removed from the room to make sure no particles deposit on it while the generator is turned of and make a false pattern on the floor. When the cardboard is on the floor, strings are put on it with a distance between each other of 20cm for the first 2m from the manikin and 50cm between each other from 2m to 3m , this is shown in figure H.1.



Figure H.1: The room before measurements.

When everything is set up, the position of manikins, the heat release of the manikins and the exhalation temperature is at a acceptable level, the ventilation system is turned of and the door to the room is closed and it is allowed to reach steady state. This usually takes two hours test have been performed in order to figure out this time period. The particle generator is turned on after two hours and the manikin exhales particles for two hours, which is enough time to make a pattern on the floor, this has also been tested prior to the measurements. After two hours are the generator turned of and the ventilation system is turned on. This is done for two reasons mainly to remove the particle so it is possible to enter the room and take pictures inside of it without inhaling to many particle but also to make sure each measurement runs for the same time period in order to be able to compare the patterns on the floor with other measurements. Pictures of the deposited particles are taken when the main part of particles are removed from the air. The sample glasses placed on the floor where the depositions of particles are greatest when acceptable pictures of the pattern on the floor are acquired this is illustrated in figure H.2.

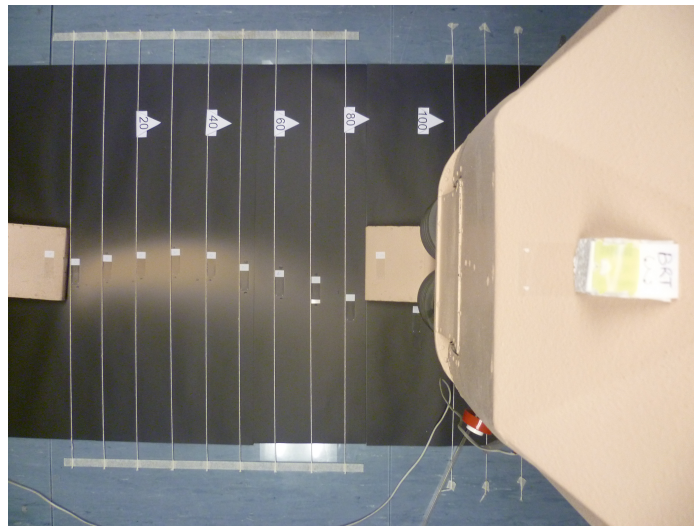


Figure H.2: The position of glasses on the floor.

Once the sample glasses are placed, are the door shut and the room is left to reach steady state again, this means no entering the room for at least two hours. The particle generator is turned on after steady state are reached inside the room.

The particle samplers have to be removed at the right time, meaning if they stay in the room for too long time too many particles will deposit on them and if they are in the room for too short time not enough particle deposit on the sample glasses. Therefore are the glasses removed at different times after starting the generator. Those closest to the manikin are removed shortly after starting the generator and further away stay in the room for longer time. If too many particles have deposited at a sampler it is impossible to analyze it with the software used to count and measure particles with. If two particles land on each other the counting software register it as one particle and if the edges of the particles are not very clear the software are not able to register that there is a border and may make it in to many small particles, this is also one of the reason why small particle are removed when analyzing the results.

Calculation on minute volume used in measurements

Since the Artificial lung does not deliver the MV that is it supposed it is calibrated. The equipment used for the calibration is not big enough to calibrate the large flows from the lung which is used in the measurements. Figure I.1 shows the measured minute volume dependent of the breathing frequency at a given fixed minute volume setting on the lung.

L/min on lung	7.5		
BF	10	15	30
Measured l/min	3.36	4.88	8.83
Relative l/min	0.45	0.65	1.18
L/min on lung	10		
BF	10	15	30
Measured l/min	4.19	6.05	10.44
Relative l/min	0.42	0.60	1.04
L/min on lung	13		
BF	10	15	30
Measured l/min	6.03	7.97	13.20
Relative l/min	0.46	0.61	1.02

Figure I.1: The particle distribution for case 1.

It is seen from figure I.1 that there is a correlation between the minute volume on the lung, the breathing frequency and the actual minute volume this is the value entered in the relative *l/min* field. A average of the three values for each breathing frequency is used when the minute volume for a given activity level were to be decided for the measurements in Hong Kong.